Electronic Supplementary Material (ESI) for Journal of Materials Chemistry C.

Supporting information for

Room-temperature phosphorescence from a purely organic tetraphenylmethane derivative with formyl groups in both solution and crystalline states

Haiyang Shu,[ab] Hua Li,[ab] Jiancheng Rao,[a] Liang Chen,[ab] Xin Wang,[ab] Xiaofu Wu,[a] Hongkun Tian,[ab] Hui Tong,*[ab] Lixiang Wang*[ab]

[a] State Key Laboratory of Polymer Physics and Chemistry, Changchun, Institute of Applied Chemistry, Chinese Academy of Sciences, Changchun 130022, China
[b] School of Applied Chemistry and Engineering, University of Science and Technology of China, Hefei 230026, China

Corresponding Author
* E-mail: chemtonghui@ciac.ac.cn; lixiang@ciac.ac.cn

Table of contents

Page

1. Experimental details

Measurements and Characterization: ^{1}H-NMR and ^{13}C-NMR spectra were measured using Bruker Avance NMR spectrometer. UV/Vis absorption spectra were measured by a Perkin–Elmer Lambda 35 UV/Vis spectrometer. Photoluminescence (PL) measurements were conducted utilizing FluoroMax-4 spectrophotometer equipped with a 150 W xenon lamp as the excitation source. The quantum yields were measured on an integrating sphere (Hamamatsu Photonics C9920-2). Fluorescence lifetimes and phosphorescence lifetimes were measured with a Horiba Scientific DeltaFlex spectrofluorometer. Fluorescence lifetime is using nanoLED-300 nm as the excitation source and repetition rate is 1.0 MHz. Phosphorescence lifetime is using spectralLED-290 nm as the excitation source and repetition rate is between 20.81 and 2.66 KHz. Gas chromatography-mass spectrometry (GC-MS) was measured with agent 5975.

Synthesis: All the materials used for the synthesis were purchased from commercial sources without further purification unless noted. p-tolualdehyde (TA) and tetra(4-bromophenyl) methane (TPM-4Br) were purchased from commercial sources. The TPM-4Br was recrystallized using acetone and *n*-hexane to obtain white needle-like crystals. TA is purified by reduced pressure distillation. Solvents for chemical synthesis were purified according to the standard procedures.

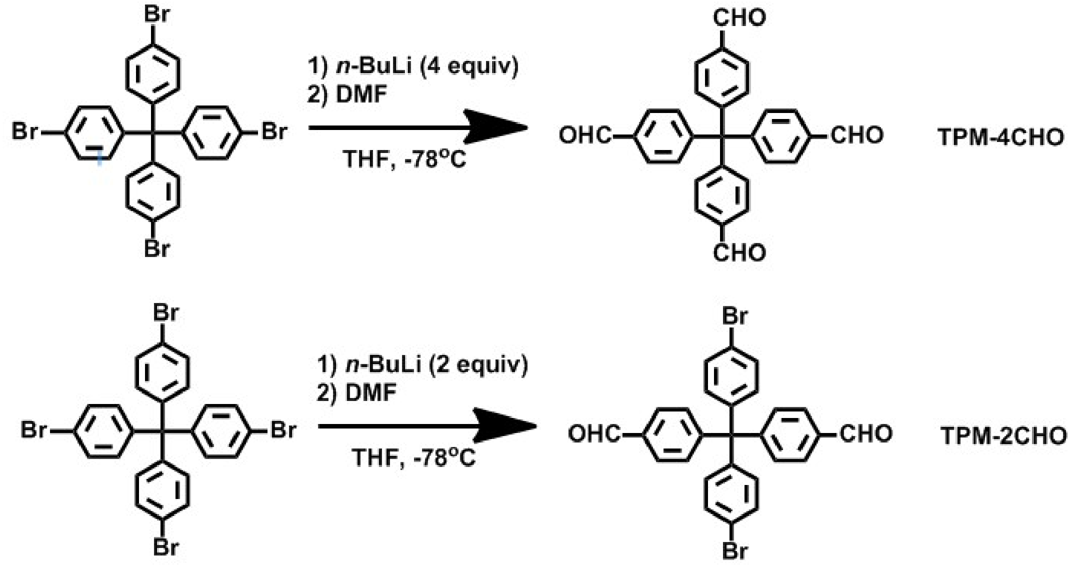

Scheme S1. Synthesis of TPM-4CHO and TPM-2CHO

Tetra(4-formylphenyl) methane (TPM-4CHO)

Tetra(4-formylphenyl) methane (TPM-4CHO) was synthesized according to a published methodology.[1] The TPM-4Br was recrystallized using acetone and *n*-hexane to obtain yellow needle-like crystals. ^{1}H NMR (500 MHz, $CDCl_3$) : δ (ppm)10.02 (s, 4H), 7.90 – 7.82 (m, 8H), 7.46 – 7.41 (m, 8H). ^{13}C NMR (126 MHz, $CDCl_3$): δ(ppm) 191.41, 151.05, 134.88, 131.24, 129.63, 66.26. GC-MS (m/z) calcd for $C_{29}H_{20}O_4$ $[M]^+$: 432.5; Found: 432.5.

4,4'-(bis(4-bromophenyl) methylene) dibenzaldehyde (TPM-2CHO)

A solution of tetra(4-bromophenyl) methane (TPM-4Br; 3.18 g, 5.00 mmol) in THF (300.00 mL) was stirred at –78 °C under dry Ar and treated dropwise with a solution of n-butyllithium (4.00 mL, 2.50 M in hexane, 10.00 mmol). The resulting mixture was kept at -78 °C for 30 min, and then DMF (0.93 mL, 12.00 mmol) was added dropwise. The mixture was stirred overnight while the temperature was allowed to rise to 25 °C. The mixture was quenched by addition of saturated NH_4Cl solution, then extracted with dichloromethane, and the combined organic phase were washed with brine, dried over $NaSO_4$, and filtered. After concentration of solvent, the residue was purified via chromatography with silica gel (petroleum ether: dichloromethane=1:2), followed by recrystallization from dichloromethane and n-hexane to afford TPM-2CHO (0.80g, 30%) as a white crystal. ^{1}H NMR (400 MHz, $CDCl_3$) δ 10.00 (s, 1H), 7.80 (d, J = 8.2 Hz, 2H), 7.61 – 7.29 (m, 4H), 7.06 (d, J = 8.5 Hz, 2H); ^{13}C NMR (126 MHz, $CDCl_3$) δ 191.50, 151.75, 143.85, 134.73, 132.33, 131.40, 131.27, 129.43, 121.19, 65.00. GC-MS (m/z) calcd for $C_{27}H_{18}Br_2O_2$ $[M]^+$: 534.0; Found: 534.0.

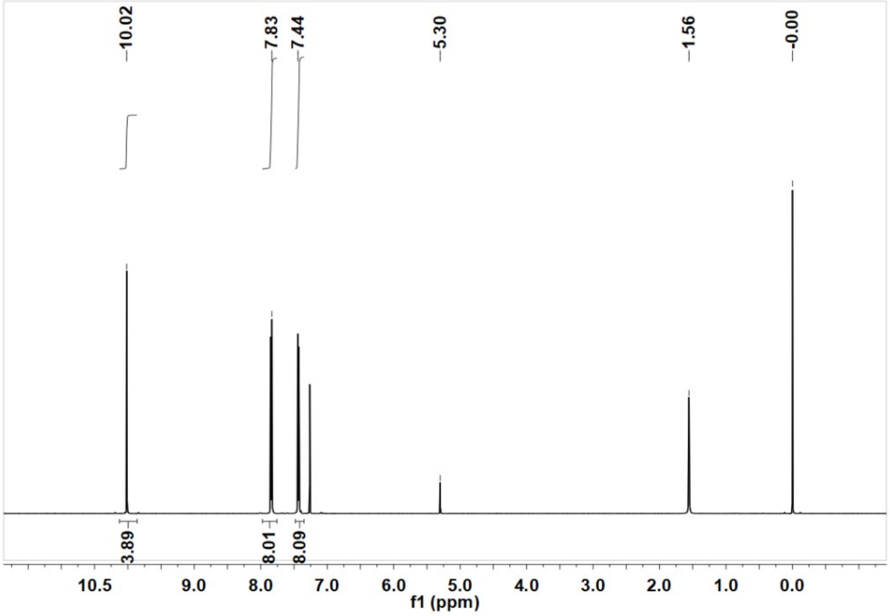

Fig. S1 ^{1}H NMR spectrum of TPM-4CHO in $CDCl_3$.

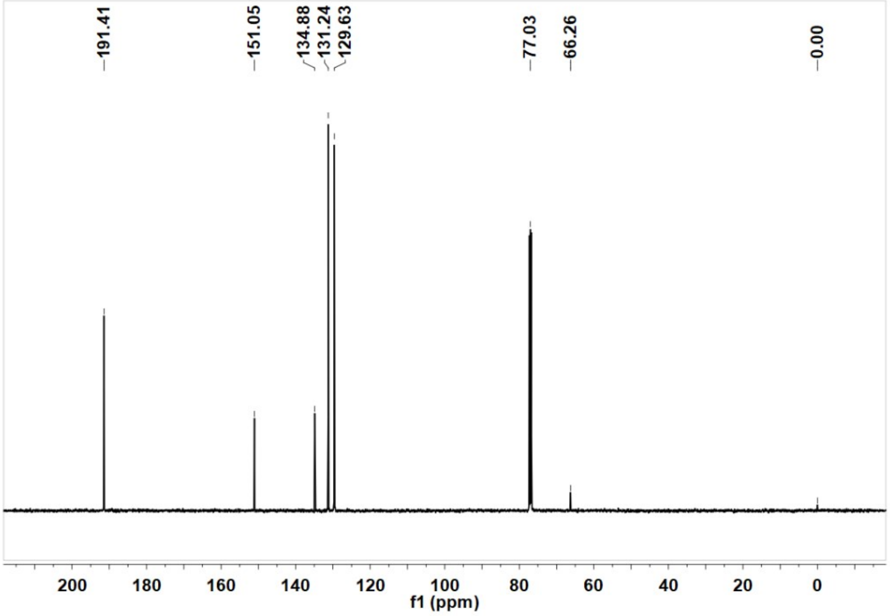

Fig. S2 ^{13}C NMR spectrum of TPM-4CHO in $CDCl_3$.

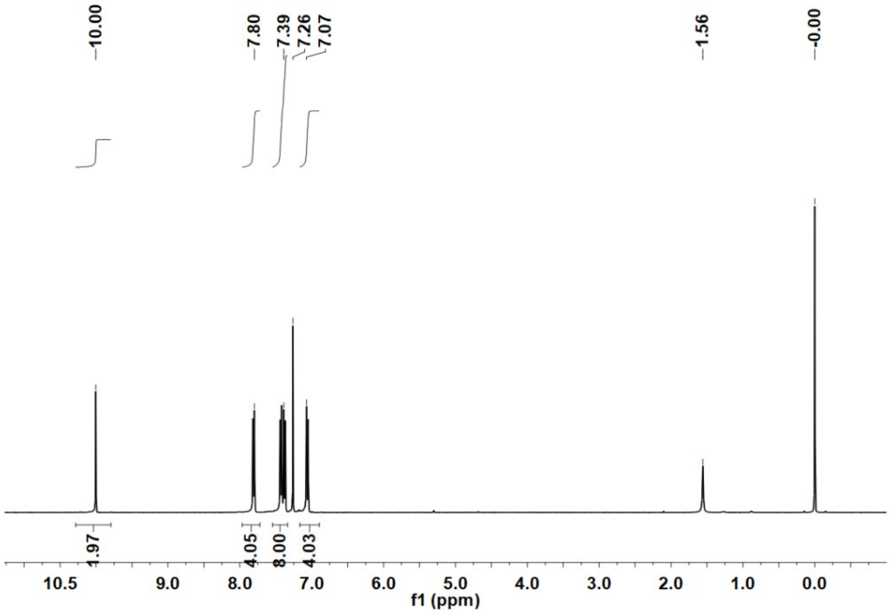

Fig. S3 ^{1}H NMR spectrum of TPM-2CHO in $CDCl_3$.

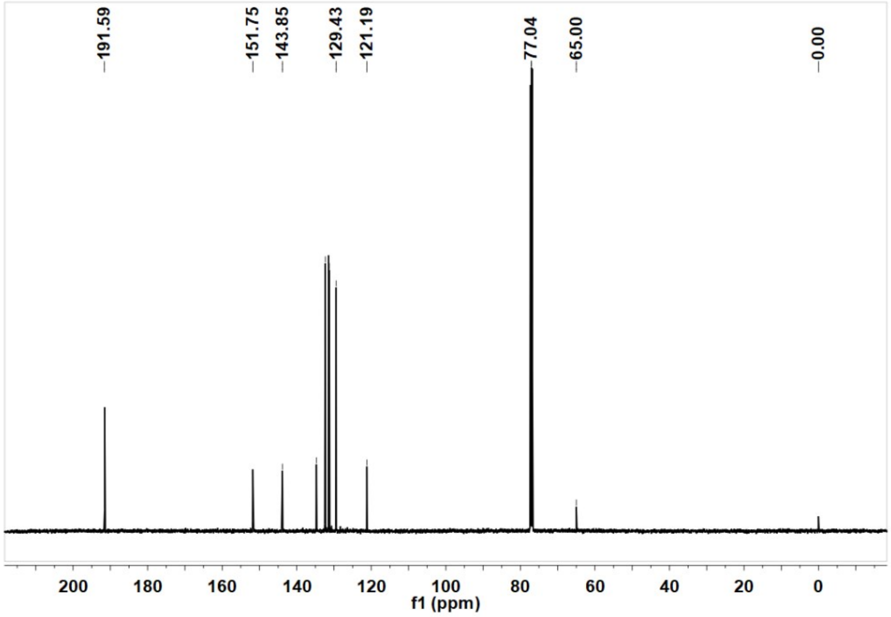

Fig. S4 ^{13}C NMR spectrum of TPM-2CHO in $CDCl_3$.

2.Photophysical measurements

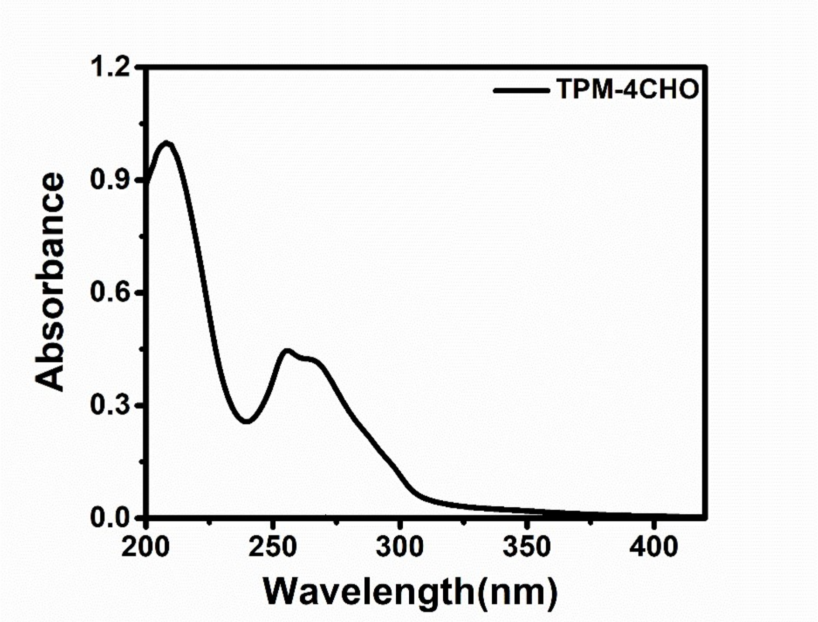

Fig. S5 UV-Vis absorption of TPM-4CHO.

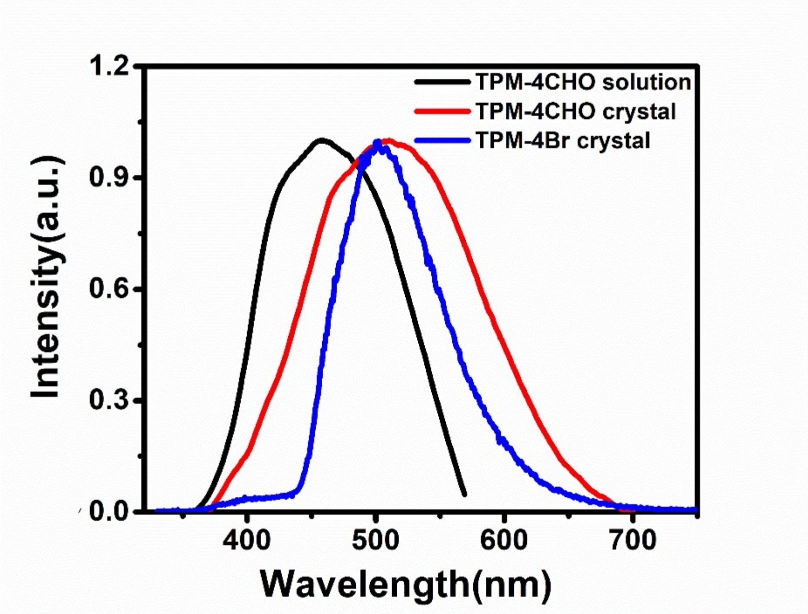

Fig. S6 Delayed emission spectra at room temperature (The delay time is 10 μs).

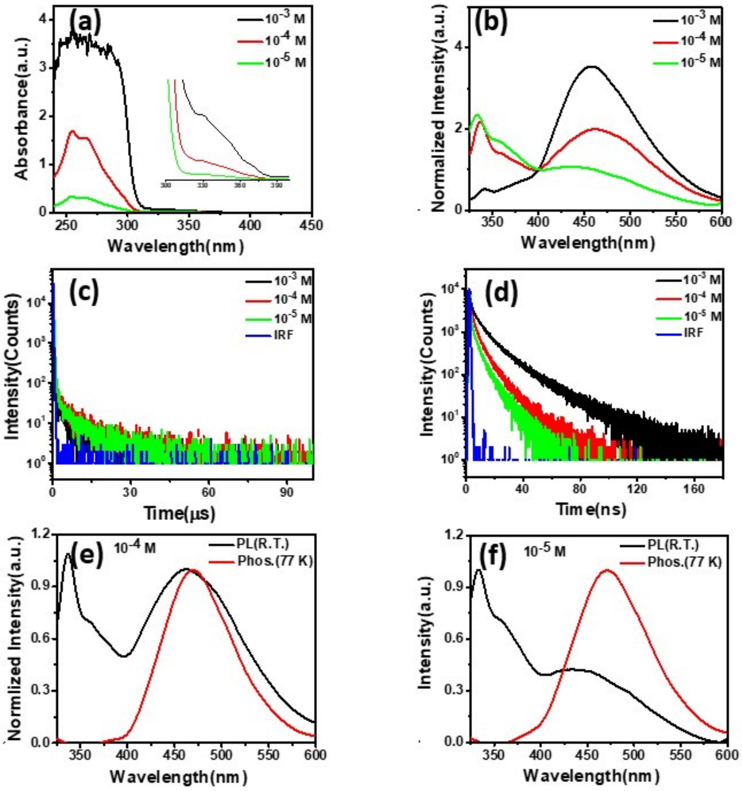

Fig. S7 (a) UV-Vis absorption (in air) (b) Steady-state spectrum (c) Phosphorescent lifetime and (d) Fluorescence lifetime of different concentrations of TPM-4CHO solution at room temperature in deareated THF; Steady-state spectra (room temperature in deareated THF) and delay spectra (77 K in air, the delay time is 10 ms) of TPM-4CHO (e) in 1.0 x 10^{-4} M and (f) in 1.0 x 10^{-5} M).

Owing to large polarity of the formyl groups, the benzaldehyde units of the TPM-4CHO will have a large dipole moment, which may result in strong intermolecular dipole-dipole force and the coexistence of monomer and dimer of TPM-4CHO even in the solution states.[2] As the concentration decreased, the ratio of dimer will reduce and that of monomer will increase. According to the theoretical calculation results, the number of intersystem crossing channels of the monomer are much less than that of the dimer, which may lead to weakened phosphorescence and enhanced fluorescence. Thus, the phosphorescence/fluorescence ratio will decrease as the solution concentration decrease. The coexistence of monomer and dimer in the solution states may also explain the bi-exponential phosphorescence decay curves. (Fig. S7c).

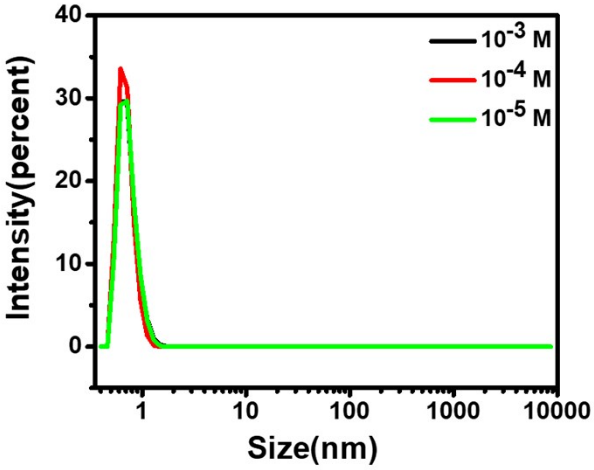

Fig. S8 Dynamic Light Scattering (DLS) measurement of different concentrations of TPM-4CHO solution.

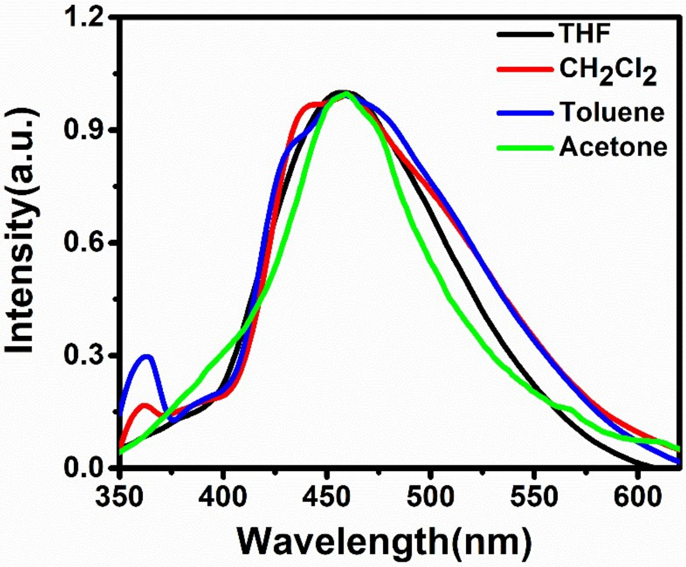

Fig. S9 RTP emission of TPM-4CHO in different solvents at room temperature.

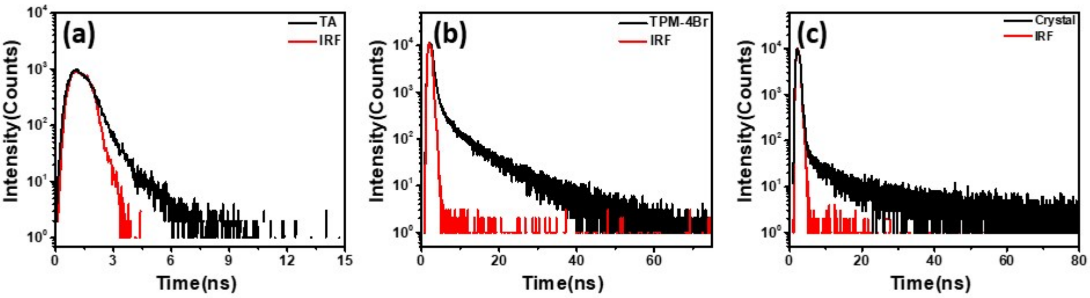

Fig. S10 Fluorescence lifetime of (a)TA in THF, (b)TPM-4Br in THF and (c)TPM-4Br crystal at room temperature and instrument response function (IRF).

Table S1. Summary of photophysical parameters at 298 K.

Compound	Fluorescence						Phosphorescence							
	λ_{FL}	τ_{avg}	τ_1	A_1	τ_2	A_2	λ_{Ph}	τ_{avg}	τ_1	A_1	τ_2	A_2	τ_3	A_3
	(nm)	(ns)	(ns)	(%)	(ns)	(%)	(nm)	(μs)	(μs)	(%)	(μs)	(%)	(μs)	(%)
TPM-4CHO	353	8.50	5.34	77	19.15	13	455	5.13	1.49	67	11.99	33	-	-
(solution)	333	2.53	1.63	88	8.78	12								
TPM-4CHO		-	-	-	-	-	509	61.67	29.08	86	11.12	14	-	-
(crystal)														
TPM-4Br	336	0.71	0.59	98	6.82	2		-	-	-	-	-	-	-
(solution)														
TPM-4Br	361	0.20	019	97	6.01	3	498	2260	230	44	2070	30	5820	26
(crystal)														
TA	338	0.38	-	-	-	-		-	-	-	-	-	-	-
(solution)														

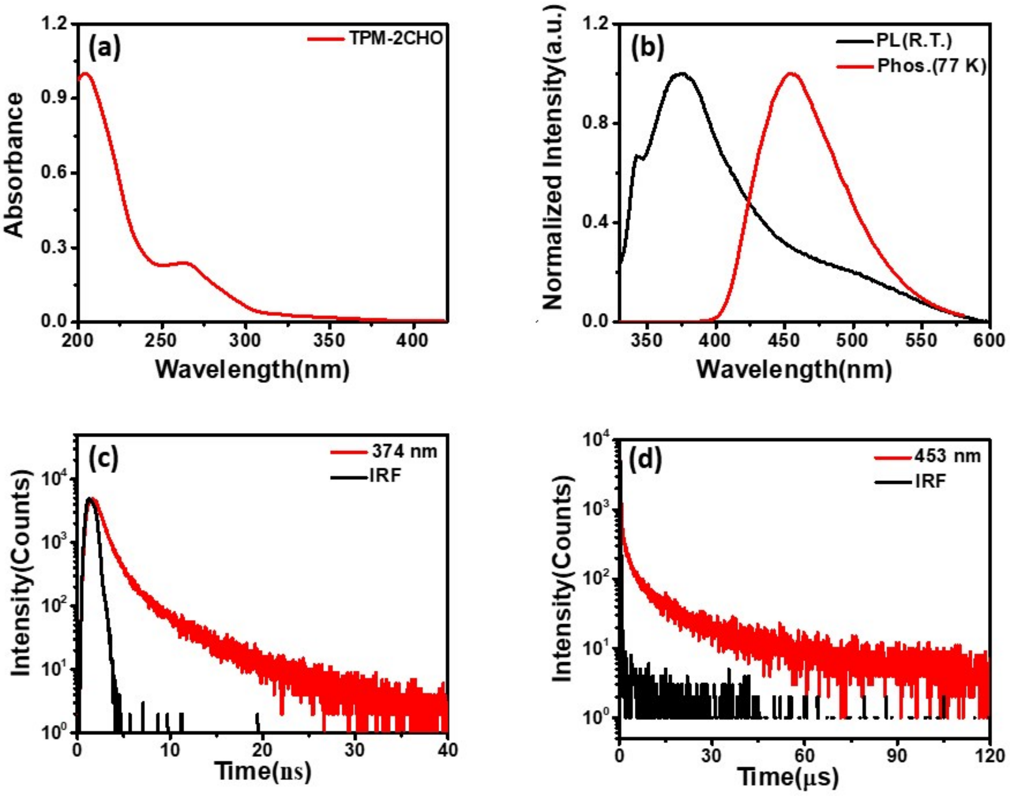

Fig. S11 (a) UV-Vis absorption (in air) (b) Steady-state spectra (room temperature in deareated THF) and delay spectra (77 K, delay time: 10 μs) of TPM-2CHO. (c) Fluorescence and (d) phosphorescence lifetime decay curves of TPM-2CHO at room temperature in deareated THF and instrument response function (IRF).

The preliminary solution data of TPM-2CHO exhibited a dominant fluorescence emission and a rather weak phosphorescence emission even in its concentrated solution (1.0 x 10^{-3} M). Its RTP emission peaked at 453 nm with the lifetime of 5.34 μs, and the phosphorescence quantum yield is only 0.2% in solution. Its fluorescence peak is at 374 nm with the emission lifetime of 1.27 ns. Compared with TPM-2CHO, TPM-4CHO with four formyl groups has higher phosphorescence/fluorescence ratio.

3. X-ray crystallographic analysis

Single crystals of TPM-4CHO was grown from acetone and *n*-hexane. The single crystal X-ray diffraction experiments were carried out using a Bruker Smart APEX diffractometer with CCD detector and graphite monochromator, Mo Kα radiation (λ =0.71073 Å). The intensity data were recorded with ω scan mode. Lorentz, polarization factors were made for the intensity data and absorption corrections were performed using SADABS program. The crystal structure was determined using the SHELXTL program and refined using full matrix least squares. All non-hydrogen atoms were assigned with anisotropic displacement parameters, whereas hydrogen atoms were placed at calculated positions theoretically and included in the final cycles of refinement in a riding model along with the attached carbons. Solvent is eliminated using the squeeze program. Thus, obtained crystallographic parameters of TPM-4CHO were summarized in Table S6 and its CCDC reference number is 1976511.

Table S2. Single crystal Data of TPM-4CHO

Name	TPM-4CHO
Empirical formula	$C_{29}H_{20}O_4$
Formula weight	432.48
Temperature	293(2)
Crystal system	Tetragonal
Space group	P4(2)/n
Unit cell dimensions	a = 13.1728 Å alpha = 90 deg b = 13.1728 Å beta = 90 deg c = 7.7112 Å gamma = 90 deg
Volume	1338.1(3)
Z	2
Density	1.073
F (000)	452.0
Radiation	Mo Kα radiation (λ =0.71073 Å)
Cell measurement theta min	3.0610
Cell measurement theta max	17.8205
CCDC	1976511

4. Theoretical calculation results

Density functional theory (DFT) and time-dependent DFT (TD-DFT) calculations were carried out at the M06-2x/6-311G** level using on Gaussian 09 package.[3] The ground state (S_0) geometry of TPM-4CHO monomer was optimized from the single crystal using solvent model. The S_0 geometry of dimer is directly optimized by single crystal. TA and TPM-4Br were directly optimized to obtain the S_0 geometry using solvent model. The calculation of TPM-4CHO monomer, TA and TPM-4Br are carried out under the solvent model. The TDDFT calculations for all molecules are performed using the optimized S_0 geometry. The orbital coupling constant (SOC) were carried out at the M06-2x/6-311G**level using on ORCA 4.1.0.[4] The SOC is calculated using optimized S_0 geometry. Relaxed potential surface energy scans of TPM-4CHO and TA were carried out at the M06-2x/6-311G** level using on Gaussian 09 package.[5] The analysis of independent gradient model (IGM) was carried out by Multiwfn 3.7 and was volume renderinged by VMD 1.9.3 based on the crystal data in initial state.[6] The single crystal of TPM-4Br comes from the literature.[7] Through the analysis of IGM, the molecular interactions can be directly displayed by the isosurface.[8]

Table S3. Energy levels of the involved singlet and triple states of TPM-4CHO (monomer)

Excited state	Energy level (eV)	Excited state	Energy level (eV)
S_1	3.7268	T_1	3.2921
S_2	3.7268	T_2	3.2921
S_3	3.7272	T_3	3.2923
S_4	3.7272	T_4	3.2924
S_5	4.8195	T_5	3.5185
S_6	4.8195	T_6	3.5185
S_7	4.9602	T_7	3.6895
S_8	4.9650	T_8	3.6929
S_9	5.0592	T_9	4.3415

Table S4. SOC of the involved singlet and triple states of a TPM-4CHO (monomer)

	SOC (cm^{-1})
$\xi(S_1, T_8)$	12.25
$\xi(S_1, T_7)$	12.35
$\xi(S_1, T_6)$	7.67
$\xi(S_1, T_5)$	1.49
$\xi(S_1, T_4)$	0.07
$\xi(S_1, T_3)$	0.06
$\xi(S_1, T_2)$	0.07
$\xi(S_1, T_1)$	0.06
$\xi(S_0, T_1)$	73.61

Table S5. Energy levels of the involved singlet and triple states of TPM-4CHO (dimer)

Excited state	Energy level (eV)	Excited state	Energy level (eV)
S_1	3.6859	T_1	3.2389
S_2	3.6859	T_2	3.2389
S_3	3.6899	T_3	3.2431
S_4	3.6899	T_4	3.2431
S_5	3.6906	T_5	3.2438
S_6	3.6906	T_6	3.2438
S_7	3.8593	T_7	3.4230
S_8	3.8619	T_8	3.4286
S_9	4.6397	T_9	3.4507
S_{10}	4.7660	T_{10}	3.4746
S_{11}	4.8658	T_{11}	3.5080
S_{12}	4.8702	T_{12}	3.5080
S_{13}	4.8855	T_{13}	3.6877
S_{14}	4.9067	T_{14}	3.7060
S_{15}	4.9494	T_{15}	3.7352
S_{16}	4.9501	T_{16}	3.7361
S_{17}	5.0355	T_{17}	4.2956

Table S6. SOC of the involved singlet and triple states of TPM-4CHO (dimer)

	SOC (cm^{-1})
$\xi(S_1, T_{16})$	3.52
$\xi(S_1, T_{15})$	2.47
$\xi(S_1, T_{14})$	8.89
$\xi(S_1, T_{13})$	5.09
$\xi(S_1, T_{12})$	0.15
$\xi(S_1, T_{11})$	0.13
$\xi(S_1, T_{10})$	10.78
$\xi(S_1, T_9)$	3.00
$\xi(S_1, T_8)$	1.13
$\xi(S_1, T_7)$	0.94
$\xi(S_1, T_6)$	0.01
$\xi(S_1, T_5)$	0.02
$\xi(S_1, T_4)$	0.02
$\xi(S_1, T_3)$	0.10
$\xi(S_1, T_2)$	0.43
$\xi(S_1, T_1)$	0.14
$\xi(S_0, T_1)$	76.73

Table S7. Energy levels of the involved singlet and triple states of TA

Excited state	Energy level (eV)	Excited state	Energy level (eV)
S_1	3.7863	T_1	3.3498
S_2	5.1486	T_2	3.6897
S_3	5.3222	T_3	4.5264

Table S8. SOC of the involved singlet and triple states of TA

	SOC (cm^{-1})
$\xi(S_1, T_2)$	19.83
$\xi(S_1, T_1)$	0.07
$\xi(S_0, T_1)$	55.44

Table S9. Energy levels of the involved singlet and triple states of TPM-4Br

Excited state	Energy level (eV)	Excited state	Energy level (eV)
S_1	5.2138	T_1	4.0966
S_2	5.2138	T_2	4.0966
S_3	5.3558	T_3	4.1234
S_4	5.3803	T_4	4.1482
S_5	5.6239	T_5	4.6854
S_6	5.6239	T_6	4.6854
S_7	5.7161	T_7	4.8037
S_8	5.7221	T_8	4.8075
S_9	5.7274	T_9	4.8405
S_{10}	5.7274	T_{10}	4.8405
S_{11}	5.8398	T_{11}	4.8502
S_{12}	6.0228	T_{12}	4.8822
S_{13}	6.1704	T_{13}	5.1647
S_{14}	6.1704	T_{14}	5.1647
S_{15}	6.2463	T_{15}	5.2110
S_{16}	6.2463	T_{16}	5.2215
S_{17}	6.2691	T_{17}	5.3461
S_{18}	6.3652	T_{18}	5.3461
S_{19}	6.3760	T_{19}	5.3468
S_{20}	6.4047	T_{20}	5.3473
S_{21}	6.4411	T_{21}	6.0959

Table S10. SOC of the involved singlet and triple states of TPM-4Br

	SOC (cm^{-1})
$\xi(S_1, T_{20})$	5.40
$\xi(S_1, T_{19})$	2.06
$\xi(S_1, T_{18})$	7.32
$\xi(S_1, T_{17})$	1.31
$\xi(S_1, T_{16})$	1.41
$\xi(S_1, T_{15})$	0.24
$\xi(S_1, T_{14})$	0.16
$\xi(S_1, T_{13})$	2.17
$\xi(S_1, T_{12})$	0.35
$\xi(S_1, T_{11})$	2.04
$\xi(S_1, T_{10})$	1.53
$\xi(S_1, T_9)$	2.53
$\xi(S_1, T_8)$	1.36
$\xi(S_1, T_7)$	1.61
$\xi(S_1, T_6)$	2.76
$\xi(S_1, T_5)$	1.69
$\xi(S_1, T_4)$	2.60
$\xi(S_1, T_3)$	0.97
$\xi(S_1, T_2)$	1.71
$\xi(S_1, T_1)$	2.56
$\xi(S_0, T_1)$	7.95

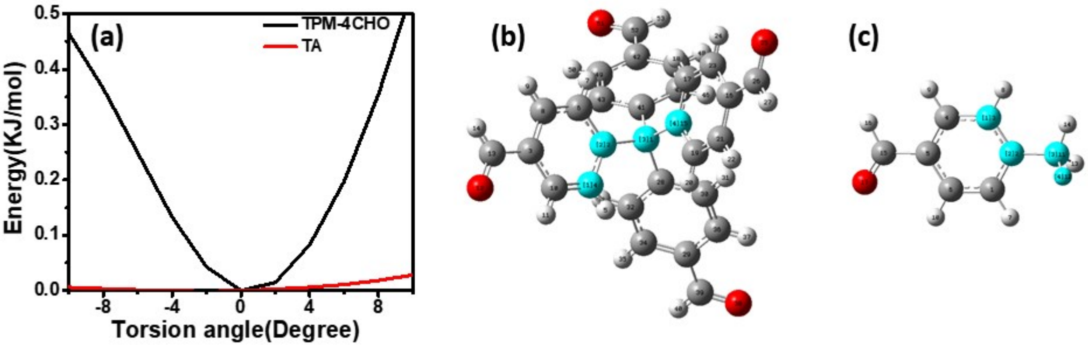

Fig. S12 Relaxed potential surface energy scans on the energy of the ground state geometry at different twisted angles.

By relaxed potential surface energy scans of TPM-4CHO and TA, the energy barriers to be overcome during the conformational change of molecules can be judged. Furthermore, the steric hindrance of the molecule can be determined. The greater the steric hindrance, the stronger the ability to suppress non-radiative transitions. The blue atoms in Fig.13b and Fig.13c are the four atoms that adjust the dihedral angle during the relaxed potential surface energy scans. In Fig.13a, 0 degree is the optimal dihedral angle, -10 degrees and 10 degrees are respectively forward and backward rotation of 10 degrees. It shows that when the dihedral angle of TPM-4CHO changes, the rate of energy rise is much greater than that of TA. This means that TPM-4CHO has a greater energy barrier to overcome during rotation, and TPM-4CHO has a stronger ability to suppress non-radiative.[5]

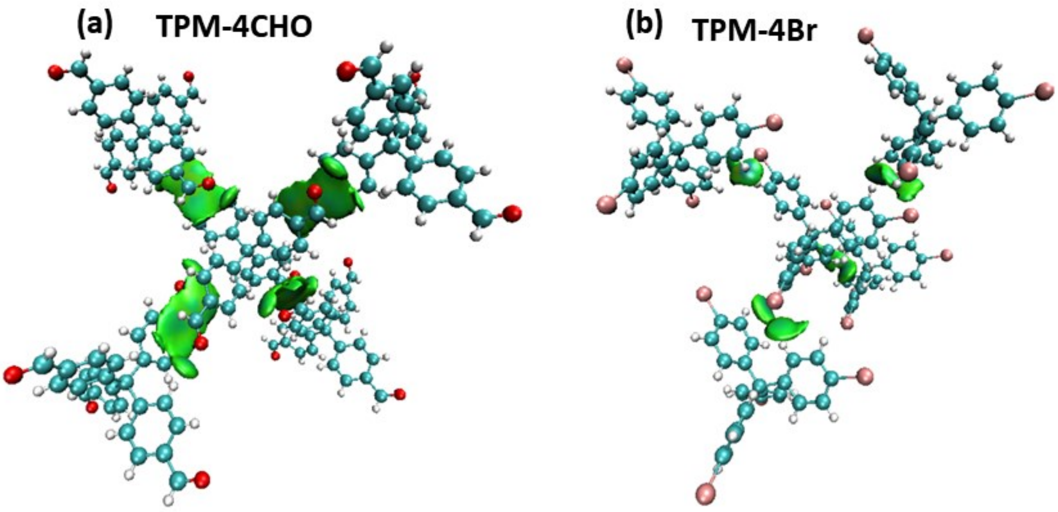

Fig. S13 The calculated molecular interactions (green isosurface) in TPM-4CHO and TPM-4Br. The isovalue is 0.003.[9]

Through IGM, the molecular interactions can be directly displayed by the isosurface in Figure S14. Obviously, TPM-4CHO has a larger isosurface. This means that TPM-4CHO has stronger intermolecular interactions. The reason is that there is a C-H···O = C hydrogen bond and n-π* interaction between the molecules of TPM-4CHO. There is only C-H···π between the molecules of TPM-4Br. TPM-4CHO suppresses non-radiative transitions more strongly.

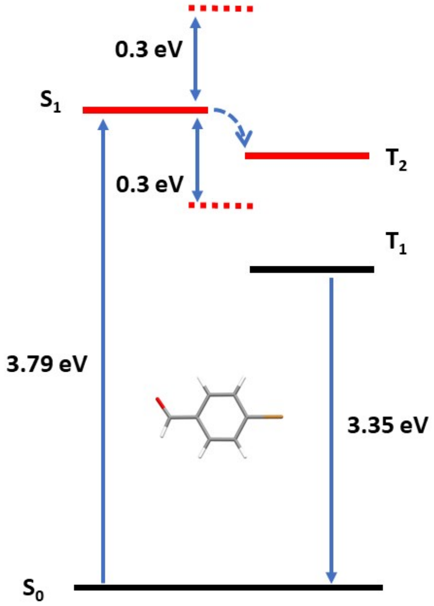

Fig. S14 Schematic diagrams showing the TD-DFT-calculated energy levels of TA at singlet (S_n) and triplet (T_n) states.

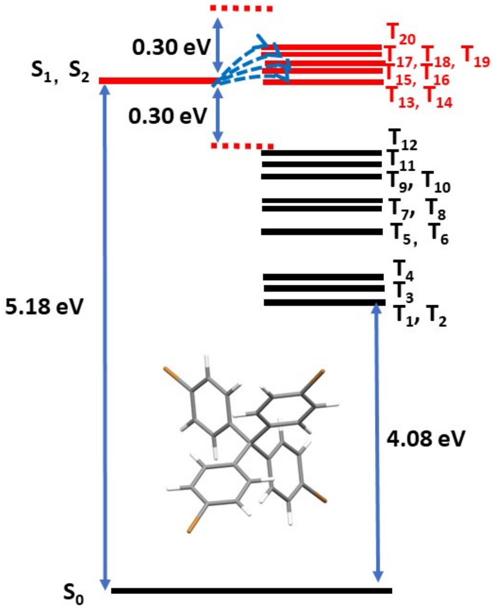

Fig. S15 Schematic diagrams showing the TD-DFT-calculated energy levels of TPM-4Br at singlet (S_n) and triplet (T_n) states.

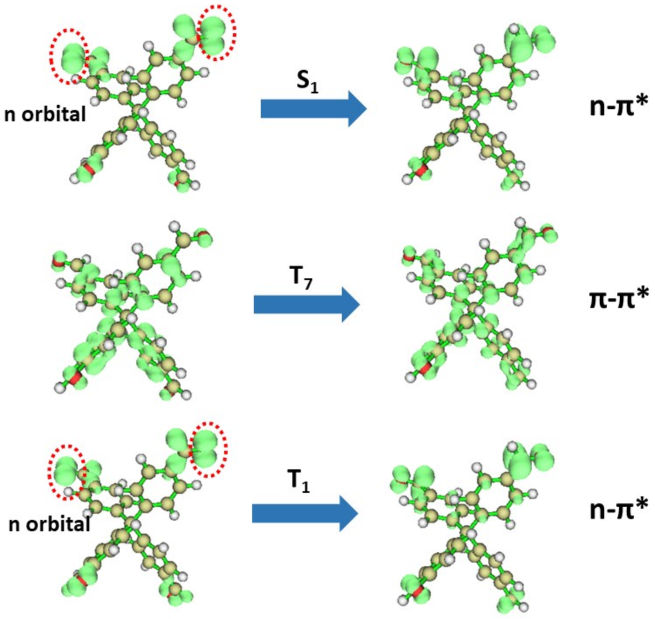

Fig. S16. Hole-electron distributions of TPM-4CHO (monomer) in different singlets (S_n) and triplet states (T_n). In the ISC (S_1-T_n) process, T_7 has the largest SOC.

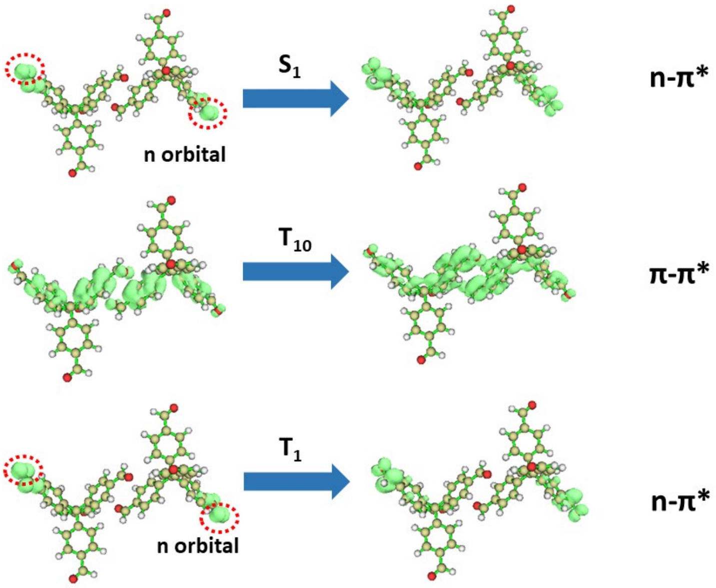

Fig. S17. Hole-electron distributions of TPM-4CHO (dimer) in different singlets (S_n) and triplet states (T_n). In the ISC (S_1-T_n) process, T_{10} has the largest SOC.

5. Reference

1. J.-H. Fournier, X. Wang and J. D. Wuest, *Can. J. Chem.,* 2003, **81**, 376–380.
2. I. Bhattacharjee, N. Acharya, S. Karmakar and D. Ray, *J. Phys. Chem. C*, 2018, **122**, 21589−21597.
3. J. Wang, X. Gu, H. Ma, Q. Peng, X. Huang, X. Zheng, S. H. P. Sung, G. Shan, J. W. Y. Lam, Z. Shuai and B. Z. Tang, *Nat Commun*, 2018, **9**, 2963.
4. M. J. Frisch, G. W. Trucks, H. B. Schlegel, G. E. Scuseria, M. A. Robb, J. R. Cheeseman, G. Scalmani, V. Barone, B. Mennucci, G. A. Petersson, H. Nakatsuji, M. Caricato, X. Li, H. P. Hratchian, A. F. Izmaylov, J. Bloino, G. Zheng, J. L. Sonnenberg, M. Hada, M. Ehara, K. Toyota, R. Fukuda, J. Hasegawa, M. Ishida, T. Nakajima, Y. Honda, O. Kitao, H. Nakai, T. Vreven, J. A. Montgomery, Jr., J. E. Peralta, F. Ogliaro, M. Bearpark, J. J. Heyd, E. Brothers, K. N. Kudin, V. N. Staroverov, T. Keith, R. Kobayashi, J. Normand, K. Raghavachari, A. Rendell, J. C. Burant, S. S. Iyengar, J. Tomasi, M. Cossi, N. Rega, J. M. Millam, M. Klene, J. E. Knox, J. B. Cross, V. Bakken, C. Adamo, J. Jaramillo, R. Gomperts, R. E. Stratmann, O. Yazyev, A. J. Austin, R. Cammi, C. Pomelli, J. W. Ochterski, R. L. Martin, K. Morokuma, V. G. Zakrzewski, G. A. Voth, P. Salvador, J. J. Dannenberg, S. Dapprich, A. D. Daniels, O. Farkas, J. B. Foresman, J. V. Ortiz, J. Cioslowski, and D. J. Fox, Gaussian 09, Revision D.01, Gaussian, Inc., Wallingford CT, 2013.
5. U. Ekstrom, L. Visscher, R. Bast, A. J. Thorvaldsen and K. Ruud, *J. Chem. Theory Comput.*, 2010, **6**, 1971-1980.
6. Y. Liu, Z. Zhang, S. Feng, M. Li, L. Wu, R. Hou, X. Xu, X. Chen and Z. Bo, *J. Am. Chem. Soc.*, 2017, **139**, 3356-3359.
7. W. Humphrey, A. Dalke and K. Schulten, *J. Mol. Graphics*, 1996, **14**, 33-38.
8. D. S. Reddy, D. C. Craig and G. R. Desiraju, *J. Am. Chem. Soc.*, 1996, **118**, 4090-4093.
9. S. Tian, H. Ma, X. Wang, A. Lv, H. Shi, Y. Geng, J. Li, F. Liang, Z. M. Su, Z. An and W. Huang, *Angew. Chem. Int. Ed.,* 2019, **58**, 6645-6649.